PHYSICAL REVIEW A **76**, 011403(R) (2007)

Photoinitiated collisions between cold Cs Rydberg atoms

K. Richard Overstreet, Arne Schwettmann, Jonathan Tallant, and James P. Shaffer*
The University of Oklahoma, Homer L. Dodge Department of Physics and Astronomy, 440 West Brooks Street, Norman, Oklahoma 73019, USA
(Received 29 March 2007; published 27 July 2007)

Experimental studies of a photoinitiated collision in an ultracold Cs Rydberg gas are presented. The process is characterized by measuring the laser intensity dependence of the absorption, the number of particles leaving each collision, and the recoil velocity of the collision fragments. The results of the experiment are compared to *ab initio* Rydberg pair interaction potentials.

DOI: 10.1103/PhysRevA.76.011403 PACS number(s): 32.80.Rm, 33.80.Ps, 34.20.Mq, 39.30.+w

Ultracold Rydberg gases are attracting increasing interest because the large polarizabilities of Rydberg atoms result in long-range tunable interactions [1–6]. Many particle effects [7–9], spontaneous ionization into an ultracold plasma [10,11], the formation of long-range Rydberg molecules [12,13], and the nonlinear optical effects that are fundamental ingredients for using cold Rydberg atoms for quantum computing [14,15] are all examples of phenomena where long-range interactions play a critical role. We present work on two-atom photoinitiated (PI) resonances in the spectrum of a cold Cs Rydberg gas that result from long-range pair interactions.

Two-photon excitation gives rise to new absorption resonances in the spectra of cold Rydberg gases [7]. Figure 1 shows two spectra of a laser-cooled Cs Rydberg gas taken over the same energy region at different laser intensities. At low intensity, only the $89D_{3/2}$ and $89D_{5/2}$ Rydberg states are observed. At high intensities, new spectral features appear. The type of resonance displayed in Fig. 1 has also been observed in cold Rb Rydberg gases and appears to be common [7]. Details of how the spectra were acquired are described in following parts of the paper.

We characterize the process associated with the absorption resonance shown in Fig. 1 and compare the experimental results to *ab initio* calculations of Rydberg pair potentials [1]. The process that gives rise to this feature is the PI and subsequent dissociation of Rydberg atom pairs. In the case studied here, 2 Cs $6P_{3/2}(F=5)$ atoms are simultaneously excited and fall apart in the $88D_{5/2}$ and $90D_{5/2}$ Rydberg states with excess kinetic energy, as in a PI collision.

The Rydberg atoms are excited from Cs prepared in a magneto-optical trap (MOT). The trapping laser is red detuned 3Γ from $6S_{1/2}(F=4) \rightarrow 6P_{3/2}(F=5)$. The MOT density is 3×10^{10} cm^{-3}.

The Rydberg atoms are excited using a two-photon scheme. The light for the first step is generated by a dye laser (Coherent 599-21) A, which is resonant with $6S_{1/2}(F=4) \rightarrow 6P_{3/2}(F=5)$ at $\lambda_A \sim 852$ nm. The frequency of A is referenced to a Cs saturated absorption cell. The laser is collimated to $\sim$1 mm, and the intensity was fixed at $I_A = 4$ mW/cm^2 to provide a constant $6P_{3/2}(F=5)$ density.

A dye laser (Coherent 699-21) B at $\lambda_B \sim 508$ nm excites atoms to $n \sim 90$ from $6P_{3/2}(F=5)$. The beam waist of laser B at the MOT is 104 ± 7 μm. The frequency of laser B is referenced to a wavemeter and an I_2 cell.

The trap light is extinguished 2.5 μs before Rydberg excitation. Laser A is gated on with a pulse width of 2.5 μs. Laser B is gated on for 1 μs so that both lasers overlap in time. The beams intersect at the MOT at 60°.

Pulsed field ionization (PFI) is used to measure Rydberg atom production. A high voltage pulse of 4 μs duration with an amplitude of 320 V is applied to field ionize the Rydberg atoms and accelerate the ions to a multichannel plate detector (MCP). The time-of-flight (TOF) signal is recorded with a multichannel analyzer. To measure TOF velocity distributions, the PFI field was chosen to minimize TOF broadening. The electric field slew rate is 5.3×10^9 V cm^{-1} s^{-1} and the amplitude is 53.2 V/cm at the MOT. The stray electric field was <20 mV/cm.

Identification of the PI collision process

$$\mathrm{Cs}(6P_{3/2}(F=5)) + \mathrm{Cs}(6P_{3/2}(F=5)) + 2h\nu \rightarrow \mathrm{Cs}(88D_{5/2}) + \mathrm{Cs}(90D_{5/2}) + (\mathrm{K.E.}) \quad (1)$$

was accomplished with three experiments. First, we measured the rate of collision events as a function of I_B to determine that two photons initiate the collision. Next, we verified

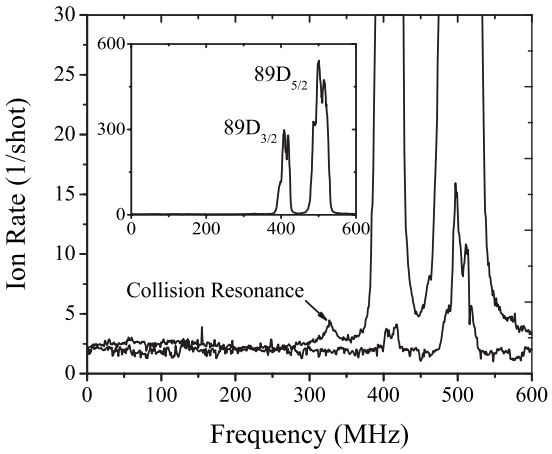

FIG. 1. Ions per laser shot vs laser B frequency. The two spectra are taken at $I_B=50$ W/cm^2 (higher yield) and $I_B=100$ mW/cm^2 (lower yield).

*shaffer@nhn.ou.edu

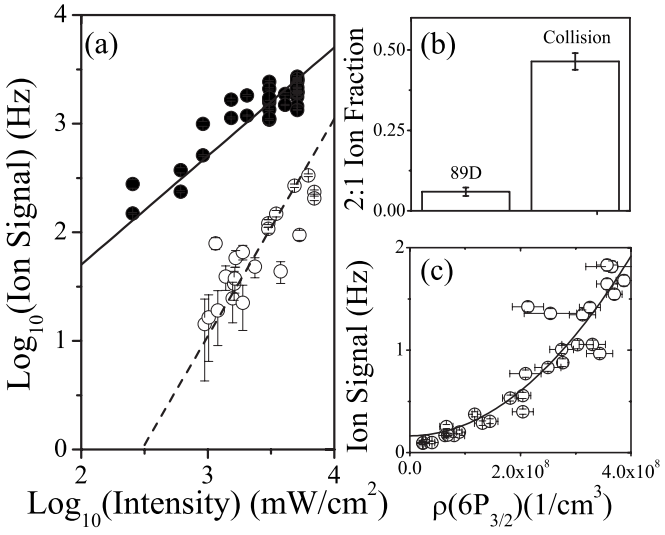

FIG. 2. (a) The peak ion production rate for $89D_{3/2}$ (solid circles) and the PI collision (open circles) vs laser B intensity at a 1-kHz repetition rate. (b) The ratio of two-ion to one-ion detections for the PI collision and $89D_{3/2}$. The 2:1 ion detection fraction for the PI collision, 0.46 ± 0.06, is in good agreement with P_D and a two-atom process. (c) The PI collision rate vs $6P_{3/2}$ density at a 30-Hz repetition rate. The line is a quadratic fit to the data.

that the collision is a two-atom process by analyzing the MCP-charge pulse-height distribution (PHD). Finally, we measured the velocity distribution of the fragments leaving the collision to determine the exit channel.

Figure 2 shows the ion rate at the peak of the PI collision and $89D_{3/2}$ resonances as a function of I_B. The ion production rate from $89D_{3/2}$ and the PI collision were measured by scanning laser B in 1-MHz steps. To minimize loss of signal due to Rydberg decay and cold plasma effects, the delay between excitation and PFI was 1 μs.

The peak ion rate for a one-photon event at low I_B scales linearly with I_B. The ion rate for a two-photon event scales as I_B^2. Consequently, a one-photon process will have slope of 1 and a two-photon process will have slope of 2 on a log-log plot of peak ion rate versus I_B. The data in Fig. 2 indicate that the PI collision is excited via two photons. Data taken for $89D_{3/2}$ have a slope of 1, as expected.

To prove the PI collision is a two-atom process, we analyzed the PHD at low I_B, when $\ll 1$ event occurs per laser shot. The charge acquired after each laser shot is proportional to the number of ions that are detected. The PHD from $89D_{3/2}$ consists of single-ion counts at low I_B. A two-Rydberg-atom process will have an increased number of two-ion detections at low I_B.

For $89D_{3/2}$, the probability of exciting n Rydberg atoms during one laser shot is determined by the binomial distribution

$$P(n) = \frac{N_{\text{atoms}}!}{n!(N_{\text{atoms}}-n)!} p_{\text{exc}}^n (1-p_{\text{exc}})^{N_{\text{atoms}}-n}, \qquad (2)$$

where p_{exc} is the probability of exciting one Rydberg atom during a laser shot. N_{atoms} is the number of available atoms. At low I_B, most laser shots will result in no excitations since p_{exc} is small. At large I_B, there will be multiple excitations. Equation (2) can also be used for a two-atom process, except now p_{exc} is the pair excitation probability and N_{atoms} the number of pairs.

The efficiency of Rydberg atom detection is decreased by decay, the quantum efficiency of the MCP, and the transmission through the MCP grid. At short PFI delay, 1 μs, essentially all of the Rydberg atoms survive. We define the Rydberg atom detection efficiency P_D as the ratio of ions detected to the number of Rydberg atoms created. The MCP quantum efficiency is $\eta \sim 60\%$ for Cs^+ at 4.5 keV [16], and the grid transmission is $t \sim 86\%$, so $P_D \sim \eta \times t = 0.52$. P_D can be taken into account using the binomial distribution for the detection process, analogous to the excitation process described by Eq. (2).

We made an independent measurement of P_D. The absorption of laser B was measured as a function of I_B to determine the number of Rydberg atoms that were excited. Laser B was frequency scanned across $89D_{3/2}$ while the trap fluorescence was monitored with a photomultiplier tube and the Rydberg atoms were ionized. The absorption rate $\gamma(I_B)$ was determined for 15 mW/cm^2 $< I_B <$ 100 mW/cm^2 using a measurement of the trap loss rate $1/\tau$ when $I_B = 0$. $\gamma(I_B) = [N - N'(I_B)]/[\tau N'(I_B)]$, where N is the steady-state atom number for $I_B = 0$ and $N'(I_B)$ is the steady-state atom number with laser B. We measured $\tau = 6.2 \pm 0.1$ s. The ion detection rate for $I_B < 4$ mW/cm^2, for count rates <100 Hz, was compared to the number of atoms that were excited according to $\gamma(I_B)$. P_D is the ion detection rate at I_B divided by $\gamma(I_B)$. $P_D = 0.47 \pm 0.06$, in agreement with the estimate.

We verified that our apparatus produced the correct PHDs when laser B was tuned to $89D_{3/2}$. We compared the PHDs for different p_{exc}. p_{exc} was varied by changing I_B. We found good agreement using Eq. (2) and P_D.

The inset of Fig. 2 shows a comparison of the fraction of two- to one-ion detections for $89D_{3/2}$ and the PI collision. These measurements were performed at 1 kHz with ion count rates of $\sim$20 Hz. The PHD for the PI collision shows an increase in the fraction of two-ion detections compared to $89D_{3/2}$. The increase in the 2:1 ion detection fraction is consistent with an overall detection efficiency of $P_D = 0.46 \pm 0.06$, in agreement with the control experiment and our estimate of P_D. The significant increase in two-ion detections and lack of three- or higher-ion detections obtained for the PI collision demonstrates that the spectral feature in Fig. 1 is a two-atom process.

To confirm the result, the MOT lasers were used to vary the density of $6P_{3/2}$ atoms via optical pumping while the PI collision ion yield was recorded, Fig. 2. The trap laser was detuned to $F = 4 \rightarrow F' = 4$, and laser A was derived from the repumping laser. The laser-B intensity was fixed. The quadratic dependence on density further shows the PI collision is a two-atom process.

Rydberg atom recoil velocity distributions were measured to identify the exit channel of the PI collision described by Eq. (1). The velocity of the fragments and the two-photon excitation energy allows us to determine the internal energy of the fragments. To measure the fragment velocities, the

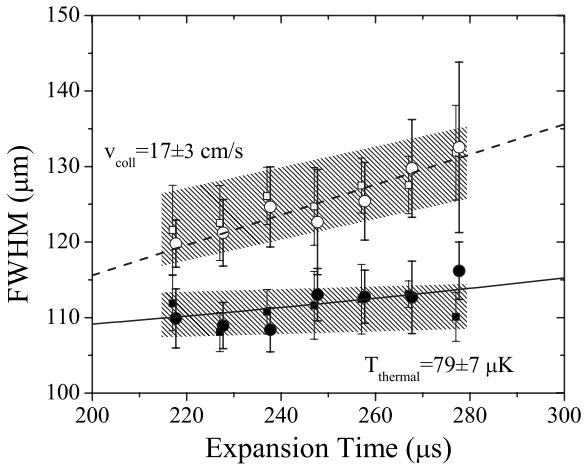

FIG. 3. The full width at half maximum (FWHM) of the fragment expansion vs expansion time. The data for the PI collision resonance and the control measurement of the temperature are shown. The lines are fits using the analysis in [17]. The small squares are the Monte Carlo data.

Rydberg atoms are allowed to expand at their thermal plus collision velocities. The expansion of the fragments is reconstructed by projecting them onto the MCP and measuring the arrival time distribution. The arrival time distribution can be converted to a velocity distribution as described in [17]. The expansion time is varied to produce enough data to determine the recoil velocity and show that the expansion does not result from ion repulsion.

The recoil velocity data are shown in Fig. 3. First, the thermal expansion of the Rydberg atoms was measured as a control by tuning laser B to $89D_{5/2}$. The temperature was 79 ± 7 μK. The recoil velocity of the atoms leaving the PI collision was measured to be 17 ± 3 cm/s. The recoil velocity and temperature are sufficiently low that the velocity distributions fit well to Gaussians. The results and uncertainties are in line with prior work [17].

The laser polarization was parallel to the TOF axis for the data in Fig. 3. The experiment was repeated with perpendicular polarization, and no difference between the two configurations was observed. The measurements suggest that the dissociation is isotropic [18,19].

The expansion time was varied by delaying the PFI pulse relative to the excitation pulse, 220–280 μs. Typical count rates were $\leqslant$100 Hz at a repetition rate of 1 kHz to minimize the number of laser shots where multiple events were initiated. $I_B=1$ W/cm^2 was held constant. The delays were chosen so that the collision exit velocity could be resolved, only one of the collision partners on average was field ionized and detected, and sufficient count rates could be obtained. Coulomb broadening will distort the TOF distribution when two Rydberg atoms ionize and repel each other during the TOF, so the experiment is set up so only one of the fragments is ionized on average and the effect of false single-ion detections is minimized.

Since the lifetime of the states around $n=90$ is $\sim$199 μs with blackbody radiation effects [20,21], a delay of 200–300 μs results in the survival of one atom $\sim$22%–32% of the time, as determined by a binomial distribution. The probability of two atoms surviving is $\sim$5%–11%. The number of single-ion detections is reduced by P_D, so $\sim$11%–16% of the single-ion detections yield the collision recoil velocity while $\sim$2.5%–5.5% of the single-ion detections, called false single-ion detections, will be influenced by ion repulsion. The remaining events result in no ion or two-ion detection. Ion repulsion leads to much larger measured velocities than recoil from the collision. For an ionization delay time of 200–300 μs and $\sim$17 cm/s recoil, the velocities due to ion repulsion are larger by more than 10 times. This increases the signal to noise, $S/N>30$ because the false single counts are spread over a larger detection time interval. Experimental evidence that indicates ion repulsion is not measured is shown in Fig. 3. Ion repulsion shows a *decrease* in FWHM as the time delay *increases*, because the fragments are ionized at larger R.

To confirm that the recoil velocity is 17 ± 3 cm/s and verify that the error is dominated by ion counting statistics, we used a Monte Carlo simulation. The number density in the excitation region, the temperature, the ion detection rate, and, for the PI collision, the exit velocity were used as input parameters. The exit velocity has fixed magnitude but random direction, since the recoil velocity distribution is isotropic.

To simulate the experiment, the initial coordinates of the atoms are picked randomly from a three-dimensional Gaussian distribution that represents the number density. Initial thermal velocities are picked from a Maxwell-Boltzmann distribution. The final distribution of atoms in space is determined for the set of delay times used in the experiment. The sample sizes used are the same as for the experiment. The FWHM of the simulated TOF distributions and error bars were compared to the ones obtained experimentally. The simulation was used to generate the confidence bands (gray region) in Fig. 3. The statistical errors from the simulation are similar to the experimental errors, providing evidence that nearly all systematic errors have been eliminated.

Calculated pair potentials [1] for $M=0$, where M is the projection of the total angular momentum along R, and an ion yield spectrum are shown in Fig. 4. The exit velocity and energy of the PI collision are consistent with dissociation along $88D_{5/2}+90D_{5/2}$. The pair potentials predict a velocity of 19 ± 4 cm/s [1]. The recoil energy and energy of the PI absorption feature agree to $<$10 MHz with $88D_{5/2}+90D_{5/2}$. The difference between the PI feature and the pair potentials is due to uncertainty in the Fabry-Perot free spectral range (±3 MHz), the I_2 spectrum (±5 MHz), the background electric field and its angular dependence (±5 MHz), and the quantum defects (at least ±3 MHz) and basis truncation (±3 MHz) used in the calculation.

The potential feature that best fits the experimental data is circled in Fig. 4. The circle highlights an inner-wall avoided crossing with a pair state correlating to $89D_{5/2}+90P_{3/2}$ that interacts strongly with $89D_{5/2}+89D_{5/2}$ at larger energies. A second avoided crossing with other states correlating to $88D_{5/2}+90D_{5/2}$ at larger R gives rise to a flat region.

The PI collision is a dissociation process where a Rydberg pair is excited. The interactions and avoided crossings are the result of the electric dipole, quadrupole-dipole, and quadrupole interactions. Unlike an electric-field-tuned resonant col-

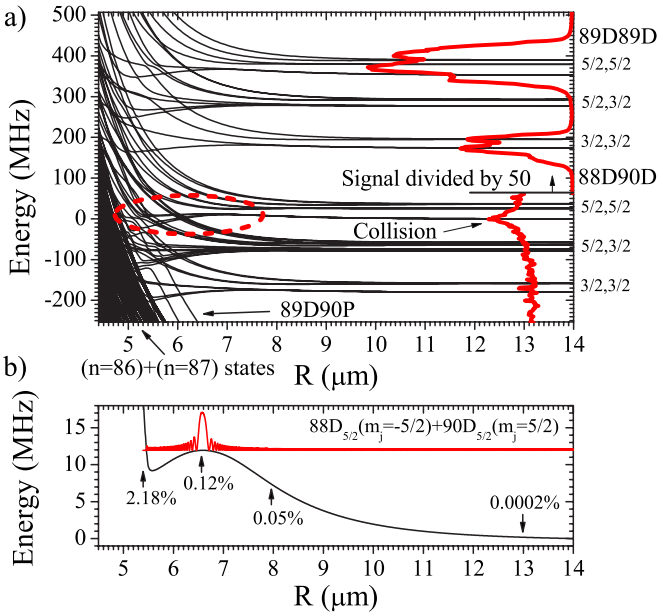

FIG. 4. (Color online) (a) Comparison of the ion yield spectra and the $M=0$ pair potentials [1]. The uncertainty in the energy of the spectra is ±10 MHz. The different asymptotes correspond to the possible m_j atomic pair states which are split by the electric field $E=20$ mV/cm. The numbers on the right refer to the j's of each atom pair state. (b) PI collision circled in (a). The percentage of 89D character, as determined from the eigenvectors [1], and the squared nuclear wave function at the top of the barrier are shown.

lision, some of the electronic energy is converted to kinetic energy. These collisions can heat the gas when a broadband laser, >0.006 cm^{-1}, excites a cold Rydberg gas.

The strength of the absorption is reduced relative to 89D by the Franck-Condon factors, the detuning from the intermediate states, and the number of pairs available. The peak PI collision count rates are more than 100 times less than the atomic states, Fig. 1. At our density, the average R is <4 μm for the $6P_{3/2}(F=5)$ atoms, so the pair distribution function is 1 for the R in Fig. 4. The contribution of $89D+89D$ to the transition at $R<7$ μm is partially responsible for the strength of the two-photon absorption, but the Franck-Condon factor is also large, ~1, because the pair potential is so flat. The intermediate states for the two-photon transition are not resonant, so the peak absorption rate is reduced.

The isotropy of the PI collision is also consistent with $88D_{5/2}+90D_{5/2}$. Each photon contributes one unit of electronic angular momentum to the two-atom complex. At the range where this process takes place, $R>4$ μm, the rotational constant is small, ~3 Hz, and the maximum rotational kinetic energy will be ~150 kHz, since the maximum nuclear angular momentum $l_{max}=\mu v R \approx 260$. Consequently, the recoil is isotropic after the process is averaged over l.

We have shown that at least some of the new spectral features that appear in a cold Rydberg gas are due to PI collisions. These PI collisions are excited via two photons. The two-photon cross sections are large because some of the potentials are unusually flat and there is a high density of Rydberg states. We compared our data to Rydberg pair potentials and found good agreement. The search for long-range Rydberg molecules will be complicated by PI collision resonances, but we showed that the recoil energy of the atoms can be used to distinguish between a dissociative and a bound state. Ion-ion recoil from a bound state will not change with PFI delay. The method that we have used to investigate this PI collision can be used in the future to study reactive processes in other cold atomic and molecular gases.

We acknowledge support from the Research Corporation and AFOSR (Grant No. FA9550-05-0328).

[1] A. Schwettmann, J. Crawford, K. R. Overstreet, and J. P. Shaffer, Phys. Rev. A **74**, 020701(R) (2006).
[2] W. R. Anderson, J. R. Veale, and T. F. Gallagher, Phys. Rev. Lett. **80**, 249 (1998).
[3] I. Mourachko *et al.*, Phys. Rev. Lett. **80**, 253 (1998).
[4] D. Tong *et al.*, Phys. Rev. Lett. **93**, 063001 (2004).
[5] K. Singer, M. Reetz-Lamour, T. Amthor, L. G. Marcassa, and M. Weidemuller, Phys. Rev. Lett. **93**, 163001 (2004).
[6] T. Cubel Liebisch, A. Reinhard, P. R. Berman, and G. Raithel, Phys. Rev. Lett. **95**, 253002 (2005).
[7] S. M. Farooqi *et al.*, Phys. Rev. Lett. **91**, 183002 (2003).
[8] W. Li *et al.*, Phys. Rev. A **70**, 042713 (2004).
[9] A. L. de Oliveira, M. W. Mancini, V. S. Bagnato, and L. G. Marcassa, Phys. Rev. Lett. **90**, 143002 (2003).
[10] T. C. Killian *et al.*, Phys. Rev. Lett. **83**, 4776 (1999).
[11] M. P. Robinson, B. Laburthe Tolra, M. W. Noel, T. F. Gallagher, and P. Pillet, Phys. Rev. Lett. **85**, 4466 (2000).
[12] C. Boisseau, I. Simbotin, and R. Côté, Phys. Rev. Lett. **88**, 133004 (2002).
[13] M. R. Flannery, D. Vrinceanu, and V. N. Ostrovksy, J. Phys. B **38**, S279 (2005).
[14] D. Jaksch *et al.*, Phys. Rev. Lett. **85**, 2208 (2000).
[15] M. D. Lukin *et al.*, Phys. Rev. Lett. **87**, 037901 (2001).
[16] J. Oberheide, P. Wilhelms, and M. Zimmer, Meas. Sci. Technol. **8**, 351 (1997).
[17] J. Tallant, K. R. Overstreet, A. Schwettmann, and J. P. Shaffer, Phys. Rev. A **74**, 023410 (2006).
[18] R. N. Zare and D. R. Herschbach, Proc. IEEE **51**, 173 (1963).
[19] M. Mons and I. Dimicoli, J. Chem. Phys. **90**, 4037 (1989).
[20] J. W. Farley and W. H. Wing, Phys. Rev. A **23**, 2397 (1981).
[21] X. He *et al.*, J. Phys. B **23**, 661 (1990).